Electronic Supporting Information

Electrochemiluminescence immunosensor based on novel heterostructured Fe-MIL-88@1T-MoS_2 dual-nanozyme with high peroxidase-like activity for sensitive NT-proBNP detection

Xinya Jiang*, Weidan Su, Wenbing Shi, Huijun Wang*,

Chongqing Key Laboratory for New Chemical Materials of Shale Gas, College of Chemistry and Chemical Engineering, Yangtze Normal University, Chongqing 408100, People's Republic of China

*Corresponding author. Tel.: +86-023-72792170; Fax: +86-023-72790008.

E-mail address: wanghj@yznu.edu.cn (H. J. Wang); jxy@yznu.edu.cn(X. Y. Jiang)

Table of contents

1.1 Reagents and apparatus

Ferric chloride hexahydrate ($FeCl_3 \cdot 6H_2O$) was purchased from Kermel Chemical Co., Ltd. (Tianjin, China). Silver nitrate ($AgNO_3$) was provided by Chengdu Chron Chemicals Co., Ltd. (Chengdu, China). Cerium nitrate hexahydrate ($Ce(NO_3)_3 \cdot 6H_2O$), ethylene glycol (EG), N, N-dimethylformamide (DMF), chitosan (CS), ammonium tetrathiomolybdate ($(NH_4)_2MoS_4$), ascorbic acid, bovine serum albumin (BSA), N-(4-Aminobutyl)-N-ethylisoluminol (ABEI), 2-aminoterephthalic acid and N-hydroxysuccinimide (NHS), N-(3-Dimethylaminopropyl)-N'-ethylcarbodiimide hydrochloride (EDC) were bought from Shanghai Titan Scientific Co., Ltd. (Shanghai, China). 2-aminoterephhalic acid (2-NH_2-BDC) was obtained from Cool Chemistry Science and Technology Co., Ltd. (Beijing, China). Polyvinylpyrrolidone (PVP, K30), hydrochloric acid (HCl), acetic acid, hydrogen peroxide (H_2O_2) were obtained from Chongqing Chuandong Chemicals Co., Ltd. (Chongqing, China). Human N-terminal pro-brain natriuretic peptides (NT-proBNP) ELISA Kit and human cardiac troponin I (cTn-I), human cardiac troponin T (cTn-T), and human myoglobin (MYO) were purchased from Nanjing Herb Source Bio-technology Co., Ltd. (Nanjing, China). Human serum was provided by the university hospital (Fuling, Chongqing). Phosphate buffered saline (PBS, pH 7.4) was composed of KCl, Na_2HPO_4 and KH_2PO_4 with the concentration of each component at 0.1 M. Throughout the study, deionized water (≥18 MΩ) was used and all the reagents (analytical grade) were used as received.

Scanning electron microscopy (SEM) images were taken by a S-4800 scanning emission microscope (Hitachi, Japan). X-ray diffraction (XRD) patterns were measured using a D8 advance power X-ray diffractometer (Bruker, Germany). Transmission electron microscopy (TEM) images were carried out with an FEI Tecnai G2 F30 electron microscope (Hillsboro, U.S.A). X-Ray photoelectron spectroscopy (XPS) data were obtained by utilizing a Thermo escalab 250XI X-ray photoelectron spectrometer. UV-vis spectra of the as-prepared nanomaterials were tested by U-3010 spectrophotometer (Hitachi, Japan). Electrochemical impedance spectroscopy (EIS) signals were performed using a CHI 660E electrochemical workstation (Chenhua, China). ECL signals were recorded on an MPI-A ECL analyzer (Remax, China) with a three-electrode system, which was composed of working electrode (glassy carbon electrode or its modified electrode), reference electrode (Ag/AgCl electrode) and counter electrode (platinum wire).

1.2 UV-vis and XPS characterization of the prepared nanomaterials

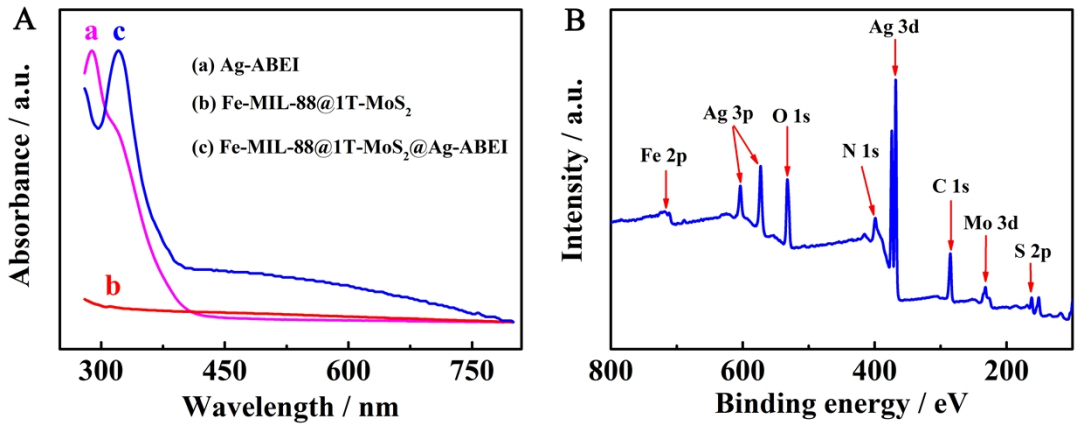

Fig. S1 UV-vis absorption spectra (A) and XPS survey (B) of Fe-MIL-88@1T-MoS_2@Ag-ABEI.

1.3 Characterization of the as-prepared ECL immunosensor

The construction process of the as-prepared ECL immunosensor was demonstrated by the electrochemical impedance spectroscopy (EIS) and ECL test, respectively. Fig. S2A was the electrochemical impedance signals of each assembly step of the immunosensor. From the figure, the CS-CeO_2/GCE (curve b) displayed a greater electron-transfer resistance (R_{et}) than the bare GCE (curve a), which was mainly due to the fact that polymer chitosan hindered electron transport. As expected, the R_{et} value of anti-NT-proBNP/CS-CeO_2/GCE (curve c) increased due to the suppression of electron transport by biological macromolecules anti-NT-proBNP. In addition, the R_{et} value of BSA/anti-NT-proBNP/CS-CeO_2/GCE (curve d) was similar to that of anti-NT-proBNP/CS-CeO_2/GCE (curve c), indicating that no redundant sites bound with BSA. Eventual, the R_{et} value of NT-proBNP/BSA/anti-NT-proBNP/ CS-CeO_2/GCE (curve e) further enhanced because of the reason that abundant biological macromolecules NT-proBNP were immobilized on electrode surface due to immune response.

Fig. S2B is the ECL signals of the as-prepared immunosensor under different conditions. In the absence of target NT-proBNP, the immunosensor showed a low ECL signal, which may be caused by the physical absorption. Nevertheless, in the presence of target NT-proBNP, the immunosensor exhibited a distinctly enhanced ECL signal as large amounts of Fe-MIL-88@1T-MoS_2@Ag-ABEI-anti-NT-proBNP-BSA bioconjugate were successfully immobilized on electrode surface *via* specific immune response. Therefore, the EIS and ECL results proved that the preparation of

ECL immunosensor was successful.

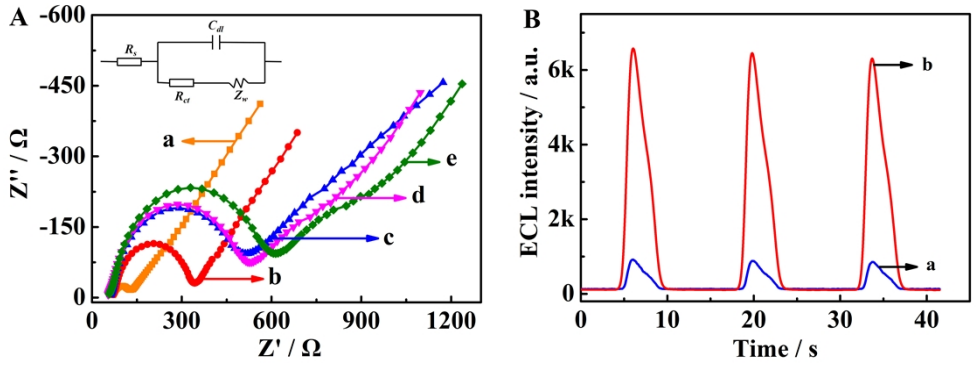

Fig. S2 (A) EIS of different modified electrodes: (a) bare GCE, (b) CS-CeO_2/GCE, (c) anti-NT-proBNP/CS-CeO_2/GCE, (d) BSA/anti-NT-proBNP/CS-CeO_2/GCE, (e) NT-proBNP/BSA/anti-NT-proBNP/CS-CeO_2/GCE. (B) ECL signals of the immunosensor under different conditions: (a) in the absence of target NT-proBNP, (b) in the presence of target NT-proBNP.

1.4 XPS characterization of hollow CeO_2 and solid CeO_2

In this work, CeO_2 was mainly used as a coreaction accelerator to accelerate the decomposition of H_2O_2 owing to its intrinsic peroxidase-like activity, which was caused by the facile redox-active Ce^{3+}/Ce^{4+} and abundant surface oxygen vacancies. The surface oxygen vacancy change can be represented by using the surface-adsorbed oxygen/lattice oxygen (O_α/O_l) ratio. Thus, in order to demonstrate that hollow CeO_2 had a superior catalytic activity, XPS characterization of hollow CeO_2 and solid CeO_2 were conducted. As showed in Fig. S3A and S3B, compared with solid CeO_2, the Ce^{3+}/Ce^{4+} content ratio on the surface of hollow CeO_2 was increased from 0.73 to 0.96, indicating that hollow CeO_2 exhibited a better catalytic activity. Furthermore, Fig. S3C and S3D also showed that the O_α/O_l ratio on the surface of hollow CeO_2 was

higher than that on the surface solid CeO_2, suggesting that hollow CeO_2 possessed more active O_α species. The increase of Ce^{3+}/Ce^{4+} content ratio and O_α/O_l ratio both indicated that hollow CeO_2 had a superior catalytic activity.

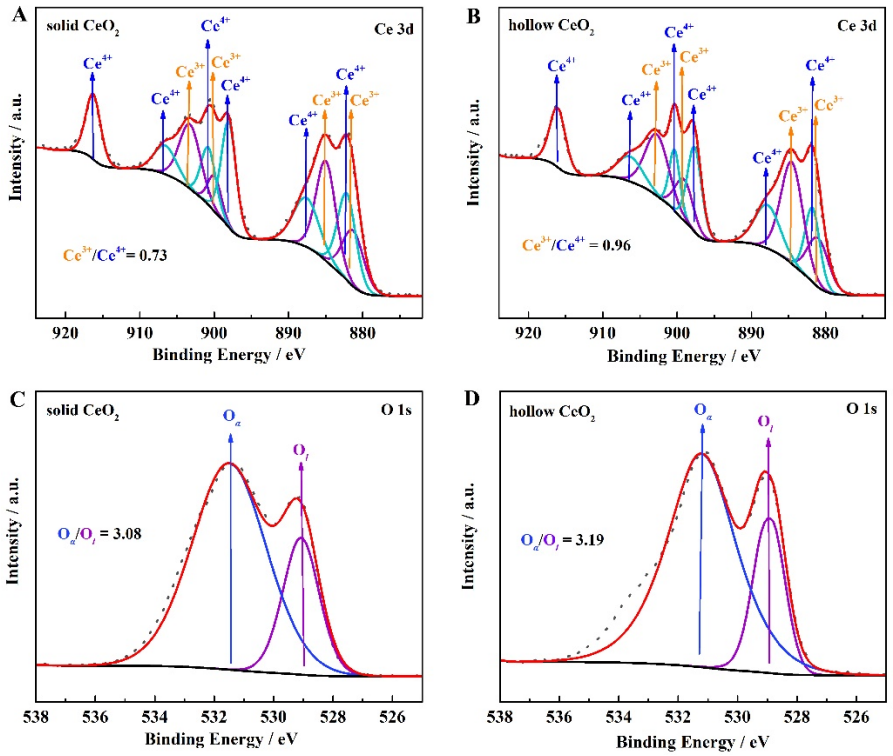

Fig. S3 Ce 3d XPS spectra of solid CeO_2 (A) and hollow CeO_2 (B). O 1s XPS spectra of solid CeO_2 (C) and hollow CeO_2 (D).

1.5 Catalytic mechanism

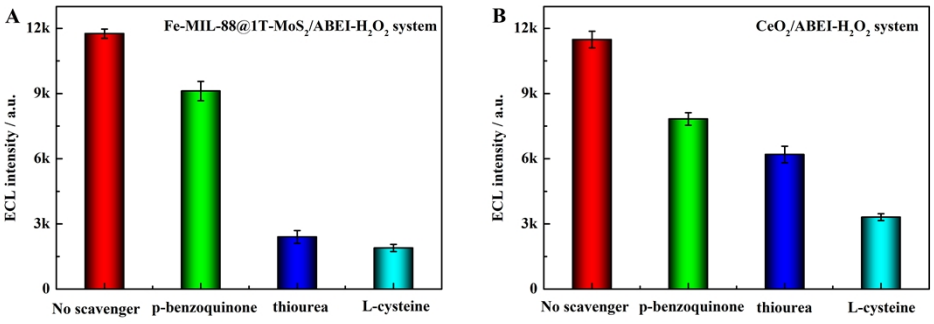

Fig. S4 The effect of p-benzoquinone, thiourea and L-cysteine on Fe-MIL-88@1T-MoS_2/ABEI-H_2O_2 (A) and CeO_2/ABEI-H_2O_2 (B) system.

1.6 Previous works for NT-proBNP detection

Table S1. Previous works for NT-proBNP detection.

Method	Detection range	Detection limit	References
SERS	/	10 pg mL^{-1}	1
FET	10 fg mL^{-1} - 1 pg mL^{-1}	41 fg mL^{-1}	2
FL	/	0.3 pg mL^{-1}	4
EIS	5 fg mL^{-1} - 1 pg mL^{-1}	5 fg mL^{-1}	4
ECL	0.5 pg mL^{-1} - 0.5 μg mL^{-1}	2.2 pg mL^{-1}	5
ECL	1 fg mL^{-1} - 100 ng mL^{-1}	0.41 fg mL^{-1}	6
ECL	1 fg mL^{-1} - 1 ng mL^{-1}	0.21 fg mL^{-1}	This work

1.7 Calculation of LOD

In this work, the LOD was calculated according to Harris' method [7]. The minimum detectable signal (I_{dl}) is expressed as follows:

$$\text{signal detection limit: } I_{dl} = I_{blank} + 3s \quad (1)$$

where s represents the standard deviation of the n measurements (n ≥ 7). The corrected signal (I_{sample} - I_{blank}) is proportional to the concetration of sample,

$$\text{calibration line: } I_{sample} - I_{blank} = m \times \text{sample concentration} \quad (2)$$

where I_{sample} is the signal detected from the sample and m represents the slope of linear calibration curve. The LOD, also called the minimum detectable concentration is calculated by substituting I_{dl} from Eq. (1) for I_{sample} in Eq. (2):

$$\text{LOD: minimum detectable concentration} = 3s/m \quad (3)$$

References:

[1] L. Wang, J. L. Sun, X. X. Wang, M. L. Lei, Z. L. Shi, L. Liu and C. X. Xu, *Talanta*, 2024, **274**, 126040.

[2] S. Jarić, A. Kudriavtseva, N. Nekrasov, A. V. Orlov, I. A. Komarov, L. A. Barsukov, I. Gadjanski, P. I. Nikitin and I. Bobrinetskiy, *Microchem. J.*, 2024, **196**, 109611.

[3] M. H. Jian, X. D. Sun, S. S. Li, H. D. Wang, H. Zhang, X. T. Li, Y. Q. He and Z. X. Wang, *Anal. Chem.*, 2024, **96**, 7353-7359.

[4] W. Ruankham, I. A. M. Frías, K. Phopin, T. Tantimongcolwat, J. Bausells, N. Zine and A. Errachid, *Talanta*, 2023, **256**, 124280.

[5] Y. Ji, S. He, Y. Chen, P. Zhang, J. Sun, Y. Li, K. D. Kuang and N. Q. Jia, *J. Mater. Chem. B*, 2023, **11**, 2754-2761.

[6] C. Wang, L. Liu, X. J. Liu, Y. Chen, X. Y. Wang, D. W. Fan, X. Kuang, X. Sun, Q. Wei and H. X. Ju, *Sens. Actuators B Chem.*, 2020, **307**, 127619.

[7] M. Saqib, S. Bashir, H. J. Li, C. P. Li, S. S. Wang and Y. D. Jin, *Anal. Chem.*, 2019, 91, 12517-12524.